Supplementary Information

Learning from human metabolism for nanomedicine: Convertible bismuth-agent for tumour-selective theranostics

Qiannan Cao,[‡a] Cuihong Yang,[‡a] Yuan Yao,[b] Bin Li,[b] Jinjian Liu,[a] Zhipeng Cao,[c] Jianfeng Liu,[a] and Meng Xiao[a]*

[a] Key Laboratory of Radiopharmacokinetics for Innovative Drugs, Chinese Academy of Medical Sciences, and Institute of Radiation Medicine, Chinese Academy of Medical Sciences & Peking Union Medical College, Tianjin, 300192, P.R. China

[b] College of Materials Science and Engineering, Qingdao University of Science and Technology, Qingdao, 266042, China

[c] School of Physics, Nanjing University, Nanjing, 210093, China

* E-mail address: xiaomeng@irm-cams.ac.cn

Chemicals and Reagents. Sodium selenite (Na_2SeO_3, 99 %), L-Buthionine-sulfoximine (L-BSO), hyaluronidase (HAase), ethylene glycol (EG, 99 %), 1-methyl-2-pyrrolidinone (NMP, anhydrous, 99.5 %), and 2',7'-dichloro-fluorescein diacetate (DCFH-DA) were purchased from Sigma-Aldrich. Glutathione (GSH) and bismuth nitrate pentahydrate ($Bi(NO_3)_3{\cdot}5H_2O$, 99 %) were purchased from Aladdin. Sodium oleate was purchased from J&K Scientific. Hyaluronan (HA) was purchased from Macklin. Cell culture mediums, penicillin, and streptomycin, fetal bovine serum, and trypsi-EDTA (0.25 %) were purchased from Gibco. Calcein-AM/PI double stain kit, DiI perchlorate and iFluor™ 555 phalloidin were purchased from Yeasen Biotechnology (Shanghai) Co., Ltd. 5,5'-Dithiobis-(2-nitrobenzoic acid) (DTNB), red Cell Proliferation, Cytotoxicity Assay Kit and GSH and GSSG Assay Kit were purchased from Beyotime Biotechnology. Hematoxylin-Eosin/HE Staining Kit and Fluorescein isothiocyanate isomer I (FITC) were purchased from Solarbio Life Sciences. 4',6-diamidino-2-phenylindole (DAPI) was purchased from Biosharp Life Sciences. FITC Annexin V apoptosis detection kit was purchased from BD Bioscience Pharmingen. Anti-gamma H2AX (phosphor A139) antibody was purchased from Abcam. Ultrapurified water was supplied by the Milli Q Plus system. BALB/c nude mice and CD rats were obtained from Beijing Vital River Laboratory Animal Technology Co., Ltd. Paraformaldehyde, sodium carbonate (Na_2CO_3), and sodium bicarbonate ($NaHCO_3$) were purchased from Heowns Biochem Technologies.LLC.TianJin. Dialysis bags (MD44-1000) were purchased from Yi bo biological.

Instruments and Characterizations. Zeta potential of surfaces of as-prepared materials were obtained by dynamic light scattering on Brookhaven, NanoBrook Omni. FTIR method was used to determine the surficial environment of the materials on BRUKER, ALPHA. UV-vis absorption spectra were measured on Persee TU-1810. Transmission electron microscopy (TEM), high resolution transmission electron microscopy (HRTEM) images and energy-dispersive X-ray spectroscopy (EDS) elemental mapping were collected on a FEI Talos F200XG2 AEMC at 200 kV accelerating voltage. X-ray photoelectron spectroscopy (XPS) characterization was performed on an ESCALAB 250XI spectrometer (Thermo Fisher, USA). X-ray powder diffraction (XRD) characterization was performed on a X'Pert PRO MPD

diffractometer with a monochromatized Cu Kα radiation source (40 kV, 40 mA). Atomic force microscopy (AFM) characterization was performed on Shimadzu, SPM-9700. A laser at 808 nm employed as the light source for in vitro and in vivo experiments was provided by Laserwave, LI-P20W. Temperature was measured through an infrared thermal imaging camera (Fluke, ST20 MAX). Photoacoustic (PA) signals of GSH-treated materials and that of tumours in vivo were detected on MOST invision 128, iThera. Fluorescence imaging of cells was operated through confocal laser scanning microscope (CLSM) on Nikon, eclipse Ti2. The apoptosis assays were analyzed on the Attune CytPix Flow Cytometer, Attune NxT. Optical absorption in hemolysis assays were detected using a Varioskan Flash multimode reader (Thermo Scientific Company, USA) at 540 nm. Histological morphology was observed through a Leica optical microscope (Leica, DMI 6000B).

Fabrication of Theranostic Precursor. Water (1 mL) and sodium oleate (100 mg) were dispersed in EG (20 mL) and kept under stirring for thorough dissolution. Then, 14 μL HNO_3 was added to prevent the hydrolysis of $Bi(NO_3)_3$, followed by the addition of 100 mg $Bi(NO_3)_3{\cdot}5H_2O$ and stirred for 2 h, during which the solution gradually changed to clear. After that, 18 mg Na_2SeO_3 was added to the flask under N_2 protection and magnetic stirring for 30 min. At last, the solution was transferred to a hydrothermal synthesis reactor and kept at 175 °C for 140 min. The final products were precipitated at a rotating speed of 8000 rpm for 5 min and washed with ethanol for six times. The obtained $Bi_2(SeO_3)_3$ NSs were dispersed in ethanol for preservation, transferred into water through three cycles of precipitation/water washing before use. For a good dispersity, specimen used in AFM measurement were obtained through dispersing the as-prepared $Bi_2(SeO_3)_3$ NSs in NMP and maintaining the system in an ultrasound field for 40 min, and this did not impact the thickness of $Bi_2(SeO_3)_3$ NSs. The theranostic precursor HA@$Bi_2(SeO_3)_3$ NSs was obtained through adding $Bi_2(SeO_3)_3$ NSs aqueous solution (0.4 mg mL^{-1}, 10 mL) into HA aqueous solution (2 mg mL^{-1}, 10 mL) and stirring for 8 h, followed with three cycles of centrifugation/water washing.

Fabrication of Fluorescent Dye-Loaded Theranostic Precursor. To prepare FITC-loaded HA@$Bi_2(SeO_3)_3$ NSs, 5 mg FITC solution (5 mg mL^{-1} in ethanol) was added into 20 mL bicarbonate buffer (0.1 M Na_2CO_3, 0.1 M $NaHCO_3$, pH = 9.5) containing 35 mg HA and kept in the dark for 24 h. Then the reaction solution was dialyzed in bicarbonate buffer for 72 h and then changed to Milli-Q water for 48 h. $Bi_2(SeO_3)_3$ NSs were wrapped with FITC-labeled HA through adding FITC-labeled HA (5 mL, 2 mg mL^{-1}) into $Bi_2(SeO_3)_3$ NSs aqueous solution (5 mL, 0.4 mg mL^{-1}) and stirring for 8 h. After dialysis in water, FITC-labeled HA@$Bi_2(SeO_3)_3$ NSs were obtained.

Evaluation of Photothermal Conversion Effect of Materials. The relationships between photothermal heating and GSH concentration, $Bi_2(SeO_3)_3$ concentration, reaction time and power density were investigated as follows. Take $Bi_2(SeO_3)_3$ NSs as an example. The volume of the reaction systems remained at 400 μL. Keep the other three variables constant, and aqueous solution of $Bi_2(SeO_3)_3$ NSs at various concentrations (0, 200, 300, 400, 600, and 800 μg mL^{-1}) reacted with GSH (11.2 mM) for 140 min separately. After 808 nm laser irradiation (1 W cm^{-2}, 10 min), temperature changes of each sample were recorded every 30 s by an IR thermal camera. Meanwhile, deionized water was used as a control under the same condition. Similarly, a) aqueous solution of $Bi_2(SeO_3)_3$ NSs (500 μg mL^{-1}) reacted with different concentrations of GSH (0, 1.2, 3.7, 7.5, 11.2, and 14.9 mM) for 140 min and the resultant solution was irradiated by laser (1 W cm^{-2}, 10 min); b) aqueous solution of $Bi_2(SeO_3)_3$ NSs (500 μg mL^{-1}) reacted with GSH (11.2 mM) for different time (0, 20, 40, 60, 80, 100, 120, 140, 160, and 180 min) and was irradiated by laser (1 W cm^{-2}, 10 min); c) aqueous solution of $Bi_2(SeO_3)_3$ NSs (500 μg mL^{-1}) reacted with GSH (11.2 mM) for 140 min and was irradiated by laser irradiation with various power densities for 10 min (0, 0.5, 1, 1.5, 2, and 2.5 W cm^{-2}).

Furthermore, in order to investigate the photostability of $Bi_2(SeO_3)_3$ NSs which reacted with GSH fully, an 808 nm laser was employed to irradiate the reacted $Bi_2(SeO_3)_3$ NSs solution (500 μL, 1.25 mg mL^{-1}) for 5 min. Cycles of laser on and off were operated for four times.

Calculation of the Photothermal Conversion Efficiency. The photothermal conversion efficiency of the converted Bi_2Se_3 NSs (Fig. S9) was calculated according to the previously reported methods.[1] The system energy balance was given as following:

$$\sum_i m_i C_{p,i} \frac{dT}{dt} = Q_{NSs} + Q_S - Q_{LOSS} \quad (1),$$

where m (g) is the mass of solvent (water), and C_p (J (g °C)$^{-1}$) is its heat capacity, T (°C) is the solution temperature, Q_{NSs} (mW) is the photothermal energy inputted by the converted Bi_2Se_3 NSs, Q_S (mW) is the baseline energy inputted by the solvent (water), and Q_{LOSS} (mW) is the energy away from the system surface to the surrounding environment.

For Q_{NSs}, Equation (2) is explained in detail:

$$Q_{NSs} = I\left(1 - 10^{-A_{808}}\right)\eta \quad (2),$$

where I represents the incident laser power (mW), A_{808} is the absorbance of the converted Bi_2Se_3 NSs at the wavelength of 808 nm, and η is the conversion efficiency from the incident light to thermal energy.

Q_{LOSS} is nearly proportional to the linear thermal driving force in this system, given by equation (3):

$$Q_{LOSS} = hS\Delta T = hS(T - T_{surr}) \quad (3),$$

where h (mW m^{-2} °C^{-1}) is the heat-transfer coefficient, S (m^2) is the surface area of the container, ΔT (°C) is the temperature change, T (°C) is the solution temperature and T_{surr} (°C) is the ambient temperature.

When the temperature rises to a maximum steady-state temperature T_{Max} °C), the heat input equals to heat output, and the left side of Equation (1) becomes zero. Then we obtain

$$Q_{NSs} + Q_S = Q_{LOSS} = hS(T_{Max} - T_{surr}) \quad (4),$$

The photothermal conversion efficiency (η) under 808 nm irradiation of the converted Bi_2Se_3 NSs was calculated by substituting Equation (2) into Equation (4) and rearranging to:

$$\eta = \frac{hS(T_{Max} - T_{surr}) - Q_S}{I\left(1 - 10^{-A_{808}}\right)} \quad (5),$$

where Q_S is measured independently to be 15.59 mW by using pure water without converted Bi_2Se_3 NSs, (T_{Max} - T_{surr}) was 42.6 °C, I is 1200 mW, A_{808} is 1.98. Thus, in Equation (5), only

hS remains unknown. In order to acquire *hS*, a dimensionless driving force temperature, θ, is introduced, using the maximum system temperature T_{Max}:

$$\theta = \frac{T - T_{surr}}{T_{Max} - T_{surr}} \quad (6),$$

Then a sample system time constant τ_s(s):

$$\tau_s = \frac{\sum_i m_i C_{p,i}}{hS} \quad (7),$$

Substitute Equation (6) and (7) into Equation (1) and rearrange to:

$$\frac{dy}{dt} = \frac{1}{\tau_s}\left[\frac{Q_{NSS} + Q_S}{hS(T_{Max} - T_{surr})}\right] \quad (8),$$

When the aqueous dispersion of the converted Bi_2Se_3 NSs was at the cooling stage, the laser was shut off. So, $Q_{NSs} + Q_S = 0$. Equation (8) can be expressed as:

$$t = -\tau_s \ln \theta \quad (9).$$

Therefore, time constant for heat transfer from the system is determined to be τ_s = 178.68 s by applying the linear time data. In addition, *m* is 384.6 mg and *C* is 4.2 J g^{-1} $°C^{-1}$. Thus, according to Equation (7), *hS* is calculated to be 4.775 mW $°C^{-1}$. Substituting *hS* into Equation (5), the photothermal conversion efficiency (η) of the converted Bi_2Se_3 NSs is calculated to be 31.1 %.

Investigation of GSH Consumption Rate. The investigation of GSH consumption rate is based on the reaction between DTNB and thiol groups, which generates TNB^{2-} with yellow color and absorption at 410 nm. Incubation of bismuth selenite (100 μg mL^{-1}) and GSH (1.5 mM) was operated in aqueous solution under 37 °C. Then 0.5 mL reaction mixture was taken out at assigned time and 0.5 mL DTNB solution (DMSO, 1.5 mM) was added. After 2 min, UV-vis spectrophotometry was conducted. GSH consumption (%) was calculated as follows:

$$GSH\ consumption\ (\%) = \frac{Abs@0\ min - Abs@assigned\ time}{Abs@0\ min - Abs@210\ min} \times 100$$

And the GSH consumption rate is the slope of the consumption curve during different period.

Cell Culture. All human breast cancer cells (MCF-7), human non-small cell lung cancer cells (A549) and mouse embryonic fibroblasts (3T3) were maintained in the DMEM medium supplemented with 10 % FBS, 1 % penicillin/streptomycin at 37 °C in a humidified atmosphere of 5 % CO_2.

Intracellular GSH Content Assay. MCF-7, A549 and 3T3 cells were separately seeded into 6 well plates at a density of 3×10^5 cells. After incubation for 24 h, HA@$Bi_2(SeO_3)_3$ NSs (100 μg mL^{-1}) was added to each well for 10, 60, and 90 min, respectively. Untreated cell samples were used as blank controls. Then the supernatants were collected and measured according to the standard protocol of the GSH and GSSG Assay Kit.

In Vitro **Photothermal Conversion Performance Evaluation.** MCF-7, A549 and 3T3 cells were separately seeded into 6 well plates at a density of 2×10^5 cells for 24 h, separately. HA@$Bi_2(SeO_3)_3$ NSs (100 μL, 400 μg mL^{-1}) were added into each well and co-incubated for 10 h. After digestion in trypsi-EDTA, the cells were collected in 200 μL PBS and exposed to laser irradiation (808 nm, 1 W cm^{-2}) for 10 min. Temperature changes of each sample were recorded every 10 s by an IR thermal camera.

Cell Viability Assay. MCF-7, A549 and 3T3 cells were separately seeded into 96 well plates at a density of 8,000 cells per well. After incubation for 24 h, samples with different concentrations of HA@$Bi_2(SeO_3)_3$ NSs (0, 3.125, 6.25, 12.5, 25, 50, 100, and 200 μg mL^{-1}) were added into each well. To investigate the biocompatibility of HA@$Bi_2(SeO_3)_3$ NSs, the relative cell viabilities were determined by Neutral Red Cell Proliferation and Cytotoxicity Assay Kit according to the standard protocol after incubation for another 24 h or 48 h.

Cellular ROS Assay. MCF-7 cells were seeded in confocal microscopic dishes at a density of 2×10^5 per well and cultured for 24 h. The cells were treated with HA@$Bi_2(SeO_3)_3$ NSs (100 μg mL^{-1}) for 24 h or 48 h. Then, the medium was discarded and the disks were rinsed by cold PBS for three times. Subsequently, oxidant-sensitive fluorescent probe DCFH-DA (10 μM, 2 mL

per well in PBS) was applied to detect ROS for 20 min at 37 °C in the dark, and fluorescent matter DCF was formed and detected by CLSM at excitation and emission wavelengths of 480 nm and 525 nm, respectively.

In Vitro **Anticancer Performance Evaluation.** Samples with different concentrations of HA@$Bi_2(SeO_3)_3$ NSs (0, 3.125, 6.25, 12.5, 25, 50, 100, and 200 μg mL^{-1}) were added to the cell medium and cultured with three types of cells for 10 h, 18 h, and 24 h. Each group (same HA@$Bi_2(SeO_3)_3$ NSs concentration and same cell type) involved three wells. NIR irradiation at 808 nm with an density of 1 W cm^{-2} were performed for 10 min. Afterwards, the cells were incubated in the dark for 10 h. Cell viability was assessed by the Neutral Red Cell Proliferation and Cytotoxicity Assay Kit according to the standard protocol.

Cellular Uptake Investigation. Cells were cultured in dishes at a density of 2×10^5 per well. After cell adhesion for 24 hours, the cells were incubated with FITC-labeled HA@$Bi_2(SeO_3)_3$ NSs (100 μg mL^{-1}) for different time periods. Afterward, the cells were rinsed with cold PBS for three times and incubated with DiI perchlorate (5 μM) at 37 °C for 20 min. Then the medium was removed and the pretreated cells were fixed with 4 % paraformaldehyde for subsequent nuclear staining with DAPI for 15 min. The cells were imaged immediately imaged by CLSM (excitation wavelengths: 405 nm, 488 nm, and 561 nm for DAPI, FITC and DiI, respectively).

Lethality Investigation. To visualize the live/dead cells, the cells were seeded in confocal microscopic dishes at a density of 3×10^5 per well and cultured for 24 h. The cells were treated with HA@$Bi_2(SeO_3)_3$ NSs (200 μg mL^{-1}) for 10 h and subsequently exposed to laser irradiation (808 nm, 1 W cm^{-2}) for 10 min. Then the cells were cultured in the dark for another 4 h and subsequently stained with calcein-AM/PI for 15 min. Finally, the labeled cells were rinsed for three times with PBS and imaged by CLSM (excitation wavelengths: 488 nm and 516 nm for calcein-AM and PI, respectively).

***γ*-H2AX Immunofluorescence Analysis.** MCF-7 cells were seeded in confocal microscopic dishes at a density of 2×10^5 per well. After cell adhesion for 24 h, the cell culture medium was replaced by a new medium containing HA@$Bi_2(SeO_3)_3$ NSs (200 μg mL^{-1}), and cultured for another 24 h or 48 h. After removing the excessive drugs, the cells were fixed by 4% paraformaldehyde for 30 min. Finally, the cells experienced classical immunofluorescence processing methods and were imaged immediately imaged by CLSM (excitation wavelengths: 405 nm and 488 nm for DAPI and FITC, respectively).

Cell Apoptosis Assay. The apoptosis assays of MCF-7 cell with different formulations were assessed *via* a FITC Annexin V apoptosis detection kit. After cultured (2×10^5/well) in 6-well plates overnight, the cells were incubated with HA@$Bi_2(SeO_3)_3$ NSs (50 μg mL^{-1}) for 24 h, 36 h or 48 h. Then, the cells were harvested, suspended in binding buffer, and stained with Annexin VFITC and propidium iodide according to the instructions. Taking cells treated with heat shock at 60 °C for 15 min as the positive control group, the samples were analyzed *via* flow cytometry.

***In Vitro* GSH Inhibition Tests.** To investigate whether photothermal effect of HA@$Bi_2(SeO_3)_3$ NSs is related to intracellular GSH, L-BSO (5 mM, 1.5 mL) was added to the cell culture medium and co-incubated with cells for 24 h in advance to inhibit the intracellular synthesis of GSH. Then HA@$Bi_2(SeO_3)_3$ NSs (200 μg mL^{-1}) was added and incubated for another 10 h, and the system was exposed to the laser irradiation (808 nm, 1 W cm^{-2}) for 10 min. Finally, CLSM was used to observe the live/dead cells directly (excitation wavelengths: 488 nm and 516 nm for calcein-AM and PI, respectively).

Cellular Morphology Investigation. MCF-7 cells receiving various treatments were employed to visualize cellular cytoskeleton morphology. These treatments include (I) PBS (control), (II) 808 nm laser irradiation, (III) co-incubated with HA@$Bi_2(SeO_3)_3$ NSs (100 μg mL^{-1}) for 10 h, (IV) co-incubated with HA@$Bi_2(SeO_3)_3$ NSs (100 μg mL^{-1}) for 10 h and exposed to 808 nm irradiation. Laser irradiation (1 W cm^{-2}, 10 min) was applied in group II and IV. After the treatments, cells were incubated in the dark for 4 h and rinsed twice with PBS. Afterwards, the

cells were labeled with Phalloidin-Alexa Fluor 555 for 1 h. The cytoskeleton morphology in various treatment groups was observed by CLSM (excitation wavelengths: 516 nm Phalloidin-Alexa Fluor 555).

Animal Use and Tumour Model Establishment. The animal use protocol has been reviewed and approved by the Animal Ethical and Welfare Committee (Assigned approval number: IRM-DWLL-2020040). All animal experiments were carried out in full compliance with the Animal Care and Use of Laboratory Animals of Peking Union Medical College. All mice were maintained in a specific pathogen-free environment. To establish MCF-7 tumour-bearing mice, MCF-7 cells were subcutaneously inoculated on several mice, and then the grown tumour was cut into tumour blocks with 1 mm^3, each of which was subcutaneously inoculated at axilla site on a new mouse. Mice will be used until the tumour volume reached 40 mm^3.

Hemolysis Analysis. Six healthy BALB/c mice (6-8 weeks) were randomized into two groups and were intravenously injected with PBS and HA@$Bi_2(SeO_3)_3$ NSs (4 mg mL^{-1}, 100 μL), respectively. Afterwards, the whole blood samples of all mice were obtained from the orbital sinus by quickly removing the eyeball from the socket after the first and seventh day to evaluate the hemocompatibility of HA@$Bi_2(SeO_3)_3$ NSs.

In the hemolysis test, red blood cells (RBCs) were obtained through centrifuging the whole blood cells of CD rat in heparinized tubes at a speed of 5,000 rpm for 5 min, followed by three times of wash with cold PBS (pH 7.4). Immediately, the RBCs were resuspended and diluted to 2 vol.% with PBS. HA@$Bi_2(SeO_3)_3$ NSs were dispersed in PBS with resultant concentrations of 0.1, 0.2, 0.4, 0.6, 0.8, 1, 2, 4, 6, and 8 mg mL^{-1}. The same volume of PBS solutions containing blood cells and HA@$Bi_2(SeO_3)_3$ NSs were added to a centrifuge tube for a total volume of 1 mL. Negative (PBS only) and positive controls (including 2 % Triton X-100) were set as references. RBCs were incubated with HA@$Bi_2(SeO_3)_3$ NSs upside down for 3 h in a 37 °C shaking water bath. Afterwards, the optical absorption of the supernatant was detected at 540 nm using a Varioskan Flash multimode reader after centrifugation (5,000 rpm, 5 min).

Hemolysis occurred when the hemolysis rate exceeded 5 %. The hemolysis rate was calculated using the following formula (where *OD* is the optical density value.):

$$Hemolysis\ (\%) = \frac{OD\ of\ sample\ absorbance - OD\ of\ negative\ absorbance}{OD\ of\ positive\ control - OD\ of\ negative\ control} \times 100$$

***In Vivo* PA Imaging Assessments.** For *in vivo* PA imaging study, MCF-7 tumour-bearing mice were intravenously injected with a dose of 40 mg kg^{-1} HA@$Bi_2(SeO_3)_3$ NSs. At varied post-injection duration (0 h, 0.5 h, 2 h, 4 h, 8 h,12 h, 24 h, and 48 h), the treated mice were anesthetized with isoflurane inhalations and the PA images of tumour regions were recorded.

***In Vivo* Anticancer Efficacy Evaluation.** MCF-7 tumour-bearing mice were randomly allocated into 4 groups (n = 5), including: (1) Control group (PBS only), (2) NIR group (irradiated by 808 nm laser at a power density of 1.0 W cm^{-2} for 10 min), (3) HA@$Bi_2(SeO_3)_3$ NSs group (intravenous injected with HA@$Bi_2(SeO_3)_3$ NSs at the dose of 20 mg kg^{-1}), and (4) HA@$Bi_2(SeO_3)_3$ NSs + NIR irradiation (intravenous injected with HA@$Bi_2(SeO_3)_3$ NSs at the dose of 20 mg kg^{-1} and 2 h later, exposed under 808 nm laser at a power density of 1.0 W cm^{-2} for 10 min). On day-0 (defined as the 10th day for tumour inoculation), mice were injected with HA@$Bi_2(SeO_3)_3$ NSs. Two hours later, the mice received PTT treatment and raised for another 21 days. Tumour volumes were measured every one day from day 0 to day 21. To evaluated the anticancer performance, the body weights and tumour volumes were monitored every other day after treatments. The tumour volume was calculated as V = (tumour length) × (tumour width)^2 / 2, and the relative tumour volume was defined as $V_R = V/V_0$ (V_0: tumour volume on the first day; V: daily-measured tumour volume). Finally, mice were sacrificed through cervical vertebra dislocation, and the vital organs (heart, liver, spleen, lung, and kidney) and tumours were excised. After weighted, tumours and other organs were fixed immediately in 4 % paraformaldehyde for the following histological analysis.

Histological Analysis. After execution, tumours and vital organs were fixed in 4 % paraformaldehyde, embedded in paraffin, and cut into pieces with a thickness of 6 μm for

pathological analysis including H&E assay according to the standard protocols. Histological morphology was observed through a Leica optical microscope.

Statistical Analysis. Concentration description are in terms of the bismuth selenite without HA encapsulation. Quantitative data were displayed as mean ± standard deviation, apart from Fig. 5e & f results as mean ± standard error of mean. Statistical comparisons were conducted using independent-samples t-test. Statistical differences were considered significant (***P < 0.001, ****P < 0.0001). SPSS 20.0 was used for statistical analysis of data.

Table S1. The t-values and degrees of freedom of involved datas.

	Data	t-value	Degree of freedom
Fig. 3a	3T3 *vs.* MCF-7	62.43	4
Fig. 3b	3T3 *vs.* MCF-7	17.65	120
Fig. 5b	Control *vs.* 0.5 h	9.793	4
	Control *vs.* 2 h	40.15	
	Control *vs.* 4 h	16.43	
	Control *vs.* 8 h	19.04	
	Control *vs.* 12 h	77.95	
	Control *vs.* 24 h	9.144	
	Control *vs.* 48 h	8.669	
Fig. 5d	$HA@Bi_2(SeO_3)_3$+NIR *vs.* PBS+NIR	6.025	40
Fig. 5e	$HA@Bi_2(SeO_3)_3$+NIR *vs.* Control	6.835	42
	$HA@Bi_2(SeO_3)_3$+NIR *vs.* NIR	6.922	
	$HA@Bi_2(SeO_3)_3$+NIR *vs.* $HA@Bi_2(SeO_3)_3$	6.895	

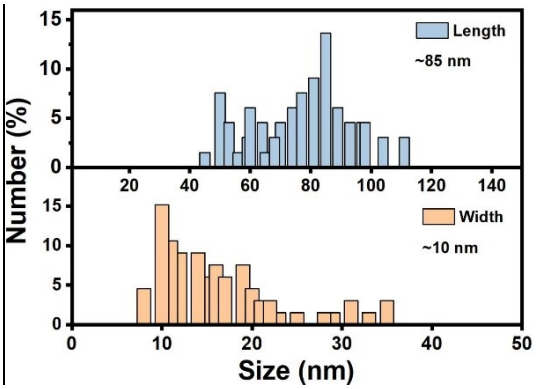

Fig. S1 Length, and width distributions determined by transmission electron microscopy results.

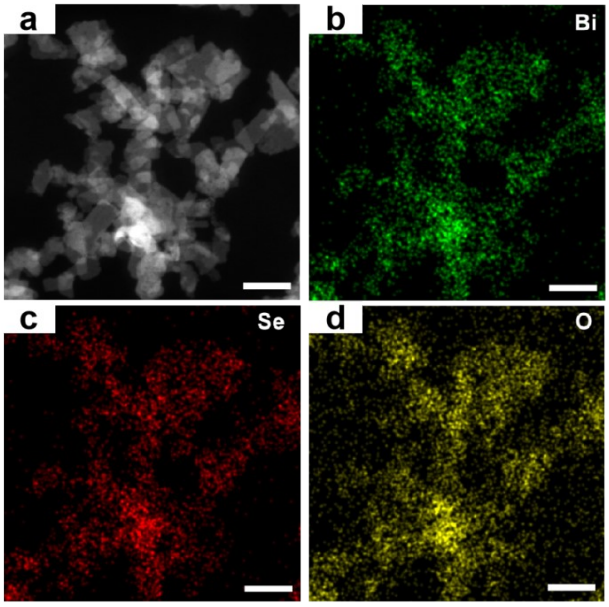

Fig. S2 EDS mapping results of the as-prepared $Bi_2(SeO_3)_3$ NSs. Scale bar = 50 nm.

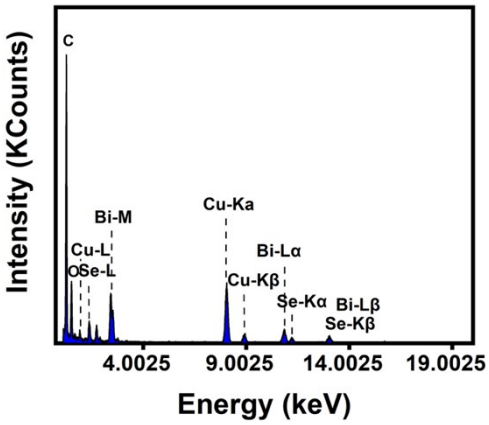

Fig. S3 EDS survey spectrum of the as-prepared $Bi_2(SeO_3)_3$ NSs.

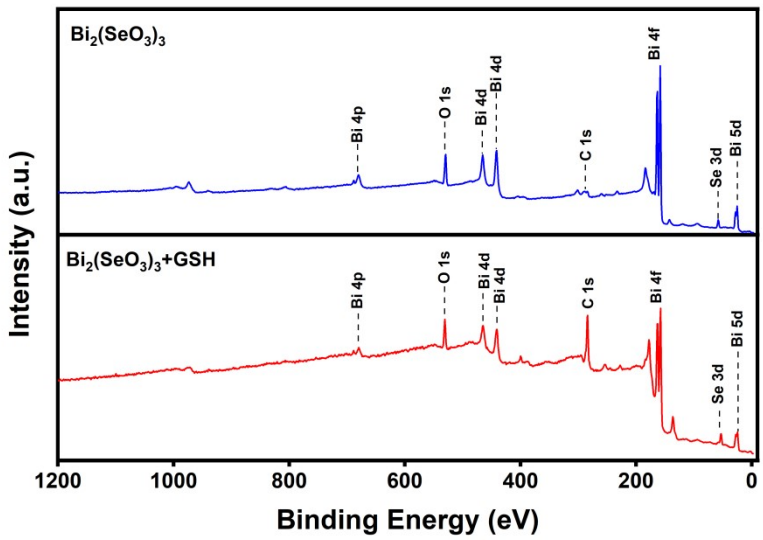

Fig. S4 XPS survey spectrum of the as-prepared $Bi_2(SeO_3)_3$ NSs.

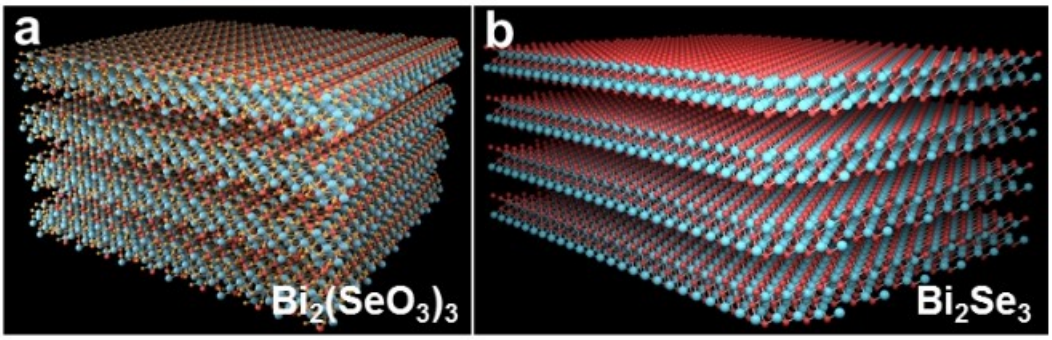

Fig. S5 The structural models of bismuth selenite and bismuth selenide, which were constructed according to TEM and XRD results and the crystallographic information file.

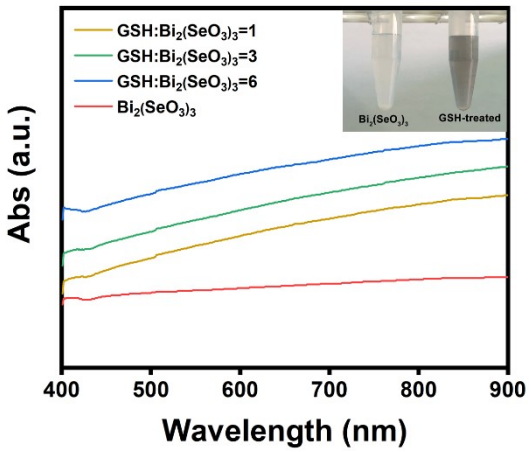

Fig. S6 Vis-NIR absorption spectra of $Bi_2(SeO_3)_3$ NSs and GSH-treated $Bi_2(SeO_3)_3$ NSs with different molar ratio, demonstrating a broad spectral response in Vis-NIR region of the converted product.

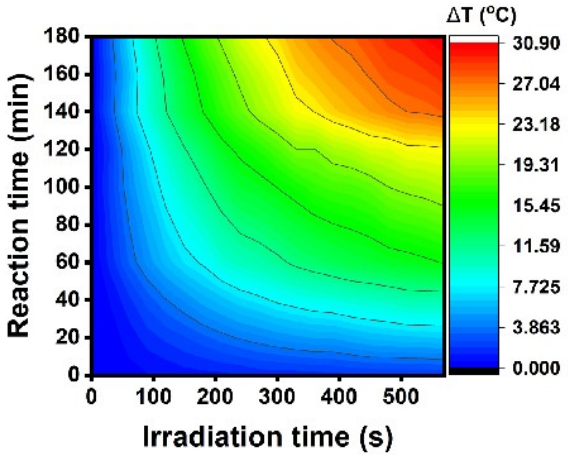

Fig. S7 Influence of reaction time on the generated heat by GSH-treated $Bi_2(SeO_3)_3$ NSs under 808 nm laser irradiation.

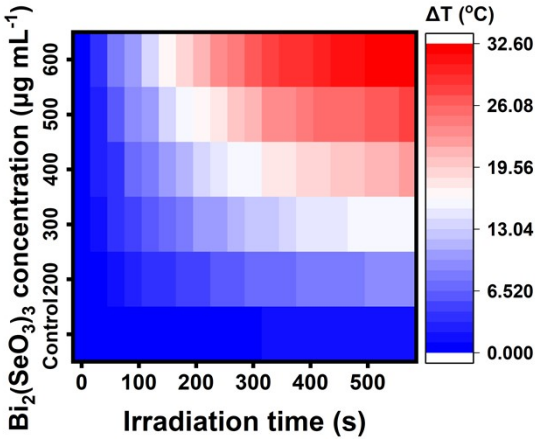

Fig. S8 Dependence of heat through photothermal conversion way on $Bi_2(SeO_3)_3$ NSs concentration under 808 nm laser irradiation.

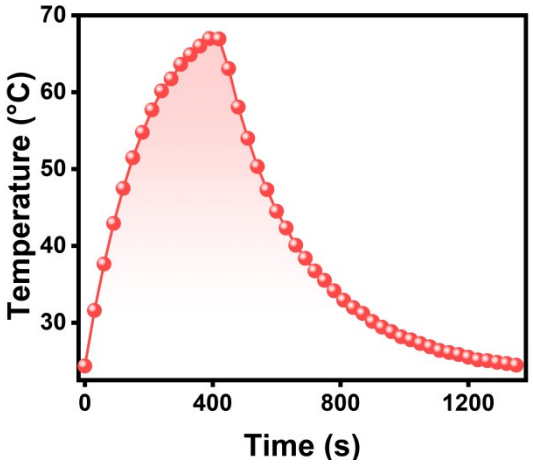

Fig. S9 Photothermal curve of GSH-treated $Bi_2(SeO_3)_3$ NSs for photothermal conversion efficiency calculation.

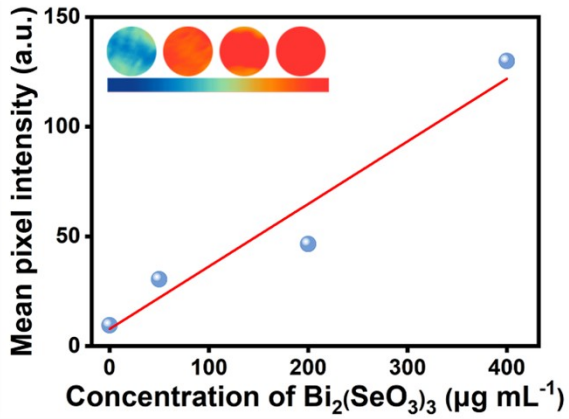

Fig. S10 *In vitro* PA imaging of the as-prepared $Bi_2(SeO_3)_3$ NSs in different $Bi_2(SeO_3)_3$ NSs concentration.

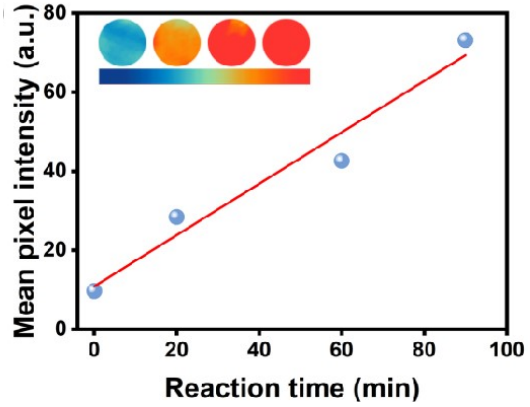

Fig. S11 *In vitro* PA imaging of the as-prepared $Bi_2(SeO_3)_3$ NSs in different reaction time.

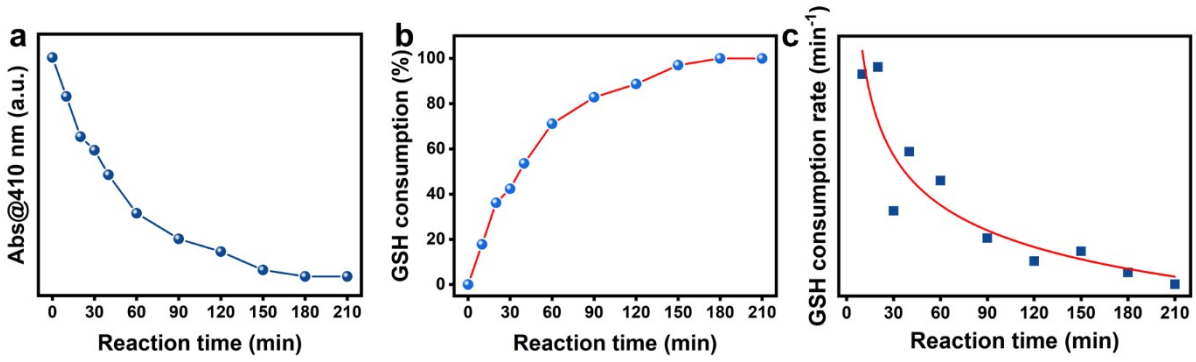

Fig. S12 GSH consumption rate determination through monitoring the residual amount of GSH in the aqueous system.

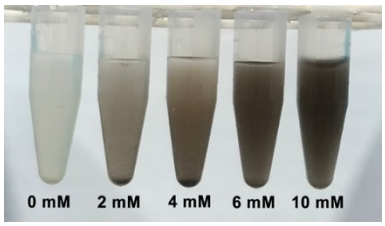

Fig. S13 Photoes of GSH-treated $Bi_2(SeO_3)_3$ NSs with different GSH concentrations. $Bi_2(SeO_3)_3$ NSs concentration was 1 mg mL^{-1}, and the reaction time was 2 h.

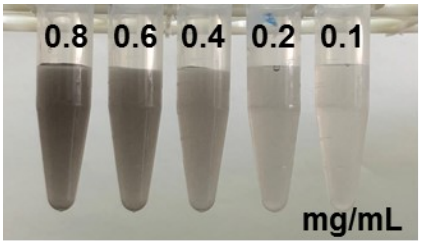

Fig. S14 Photoes of GSH-treated $Bi_2(SeO_3)_3$ NSs with different $Bi_2(SeO_3)_3$ concentrations. GSH concentration was 6 mM, and the reaction time was 3 h.

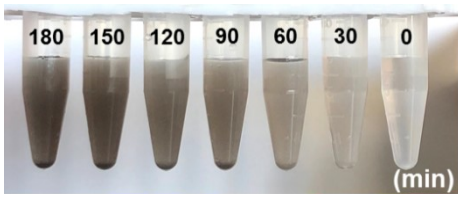

Fig. S15 Photoes of GSH-treated $Bi_2(SeO_3)_3$ NSs with different reaction time. $Bi_2(SeO_3)_3$ NSs concentration was 1 mg mL^{-1}, and GSH concentration was 6 mM.

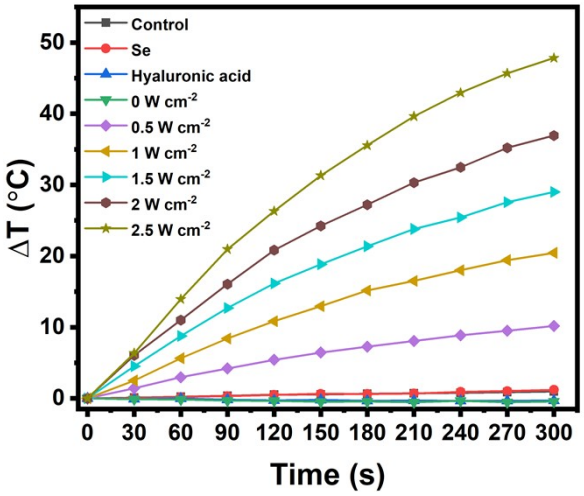

Fig. S16 Dependence of the generated heat on irradiation power intensity under 808 nm laser irradiation.

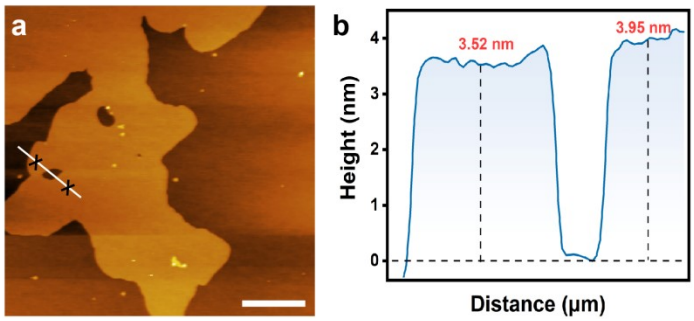

Fig. S17 AFM image of GSH-treated $Bi_2(SeO_3)_3$ NSs. Scale bar = 1 μm.

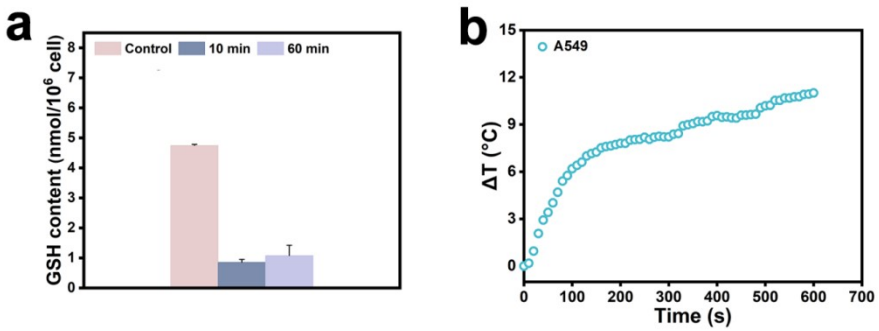

Fig. S18 a) GSH content of A549 cells in different time while incubated with $Bi_2(SeO_3)_3$ NSs and b) the corresponding temperature variation after 10 h co-incubation.

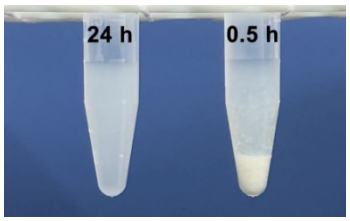

Fig. S19 Stability investigation of $Bi_2(SeO_3)_3$ NSs before (right) and after (left) HA (1 mg mL^{-1}) encapsulation.

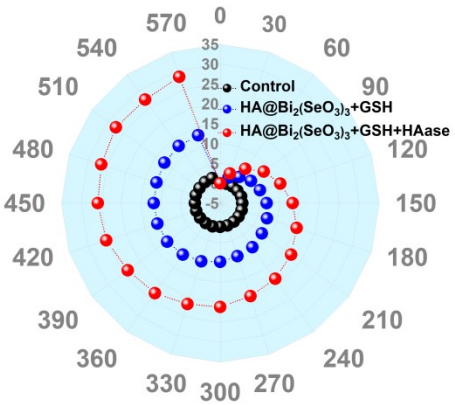

Fig. S20 Temperature variation of the system with or without HAase to dissociate the wrapped HA outside $Bi_2(SeO_3)_3$ NSs.

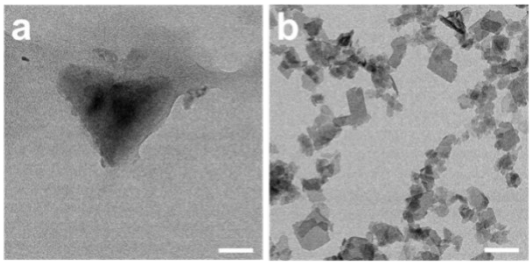

Fig. S21 TEM images of the as-prepared a) HA@$Bi_2(SeO_3)_3$ NSs and b) HAase-treated HA@$Bi_2(SeO_3)_3$ NSs. Scale bar = 50 nm.

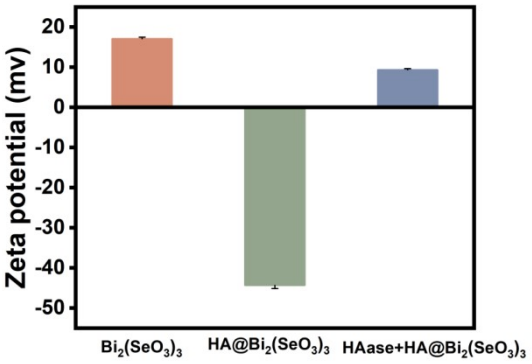

Fig. S22 Zeta potential of surfaces of $Bi_2(SeO_3)_3$ NSs, HA@$Bi_2(SeO_3)_3$ NSs and hyaluronidase-treated HA@$Bi_2(SeO_3)_3$ NSs.

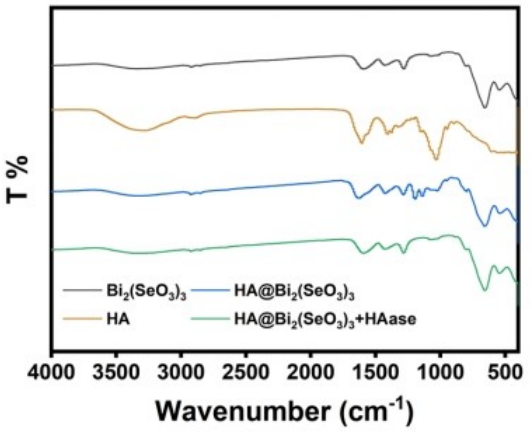

Fig. S23 FTIR results of $Bi_2(SeO_3)_3$ NSs, HA, HA@$Bi_2(SeO_3)_3$ and HA@$Bi_2(SeO_3)_3$ NSs + HAase. Peaks located at 1270−1100 cm^{-1} reveals the HA coating state on $Bi_2(SeO_3)_3$ NSs surface. The peaks appeared after $Bi_2(SeO_3)_3$ NSs were modified with HA through electrostatic interaction, while disappeared after HAase treatment.

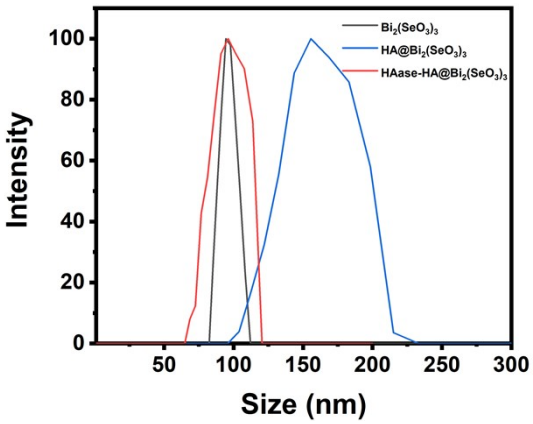

Fig. S24 Hydrodynamic sizes of the as-prepared $Bi_2(SeO_3)_3$ NSs, HA@$Bi_2(SeO_3)_3$ NSs, and HAase-treated HA@$Bi_2(SeO_3)_3$ NSs.

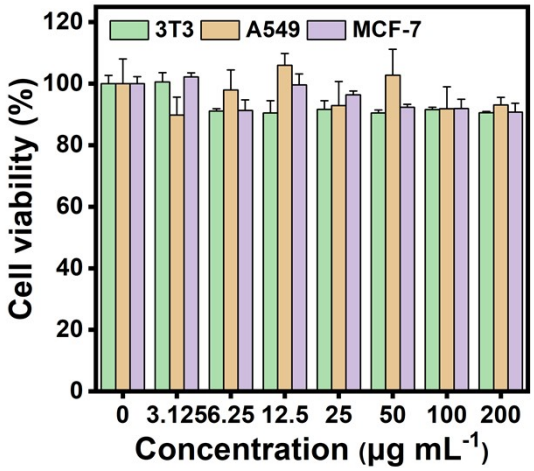

Fig. S25 Cell viability after 24 h incubation with HA@$Bi_2(SeO_3)_3$ NSs at different concentration.

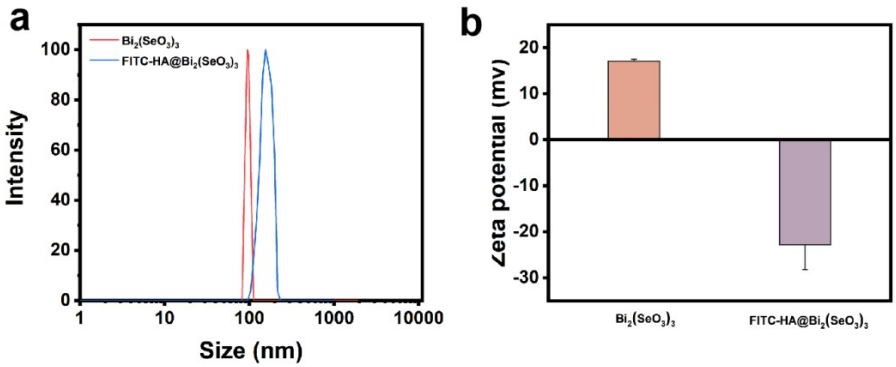

Fig. S26 a) Hydrodynamic diameters and b) zeta potential determination of the asprepared fluorescence-labelled HA@$Bi_2(SeO_3)_3$ NSs.

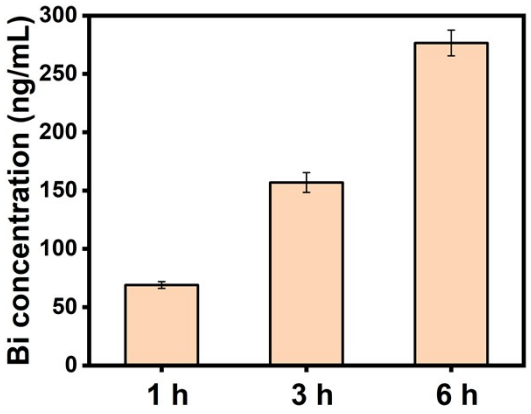

Fig. S27 ICP-MS results of bismuth element inside cancer cells after different incubation time.

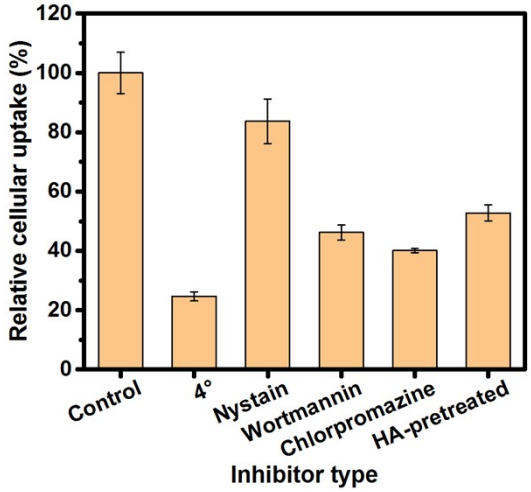

Fig. 28 ICP-MS results of bismuth element inside cancer cells after co-incubation with different cellular internalization inhibitors.

To determine the possible pathway leading towards the rapid uptake of HA@$Bi_2(SeO_3)_3$ NSs, we introduced corresponding inhibitors into the co-culture system of MCF-7 cells and HA@$Bi_2(SeO_3)_3$ NSs, and quantified the internalized bismuth element inside cells. According to the results shown in Fig. S28, the cellular uptake efficiency of HA@$Bi_2(SeO_3)_3$ NSs is significantly reduced by 4°, which indicates the internalization of HA@$Bi_2(SeO_3)_3$ NSs by cells is an energy-dependent process. The addition of wortmannin (an inhibitor of micropinocytosis) and chlorpromazine (an inhibitor of clathrin-mediated endocytosis) effectively reduced the endocytosis to 46.2% and 40.1%, respectively, compared with the cells without inhibitors. Nystatin (an inhibitor of caveolae/lipid-mediated endocytosis) decreased the cellular uptake of HA@$Bi_2(SeO_3)_3$ NSs to 83.6%, much less effective than the former ones. It can be inferred from these results that the endocytosis process of nanosheets is a multiple-effect process, in which micropinocytosis- and clathrin-mediated endocytosis may be the leading ones. More importantly, the pretreatment in HA solution effectively reduced the efficiency of cellular

uptake of HA@$Bi_2(SeO_3)_3$ NSs to 52.7%, indicating that the CD44 receptor-mediated endocytosis also plays an important role in the cellular uptake of HA@$Bi_2(SeO_3)_3$ NSs.

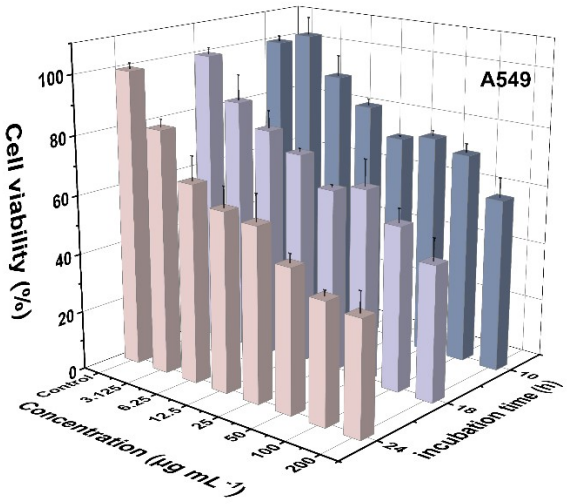

Fig. S29 Cell viability of A549 cells incubated with HA@$Bi_2(SeO_3)_3$ NSs at different concentration and incubation time (10 h, 18 h, and 24 h) and irradiated by 808 nm laser irradiation (1 W cm^{-2}, 10 min). n = 3.

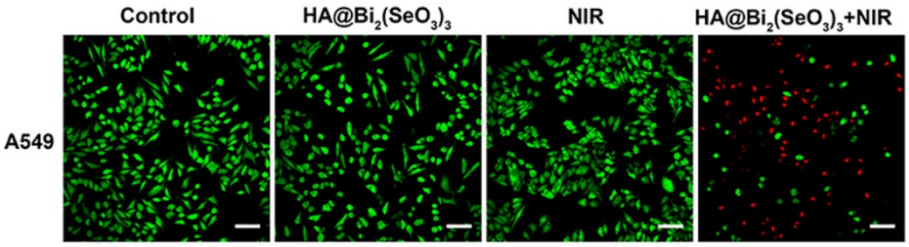

Fig. S30 Fluorescence images of live/dead cells after different treatments stained with calcein-AM and propidium iodide by confocal laser scanning microscopy. Scale bar = 100 μm.

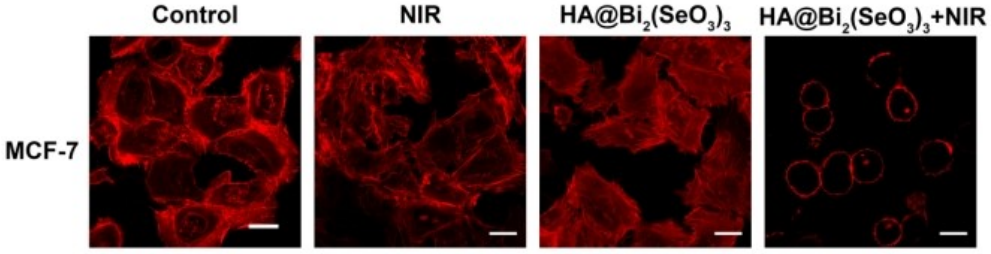

Fig. S31 CLSM images of the cellular skeleton demonstrating the severe deformation of actin filaments. Scale bar = 20 μm.

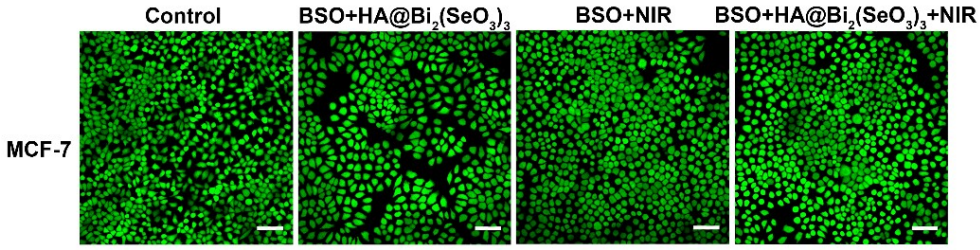

Fig. S32 Visualized demonstration of the key role of GSH in the photothermal conversion process with or without L-BSO as inhibitor of GSH synthesis. Scale bar = 100 μm.

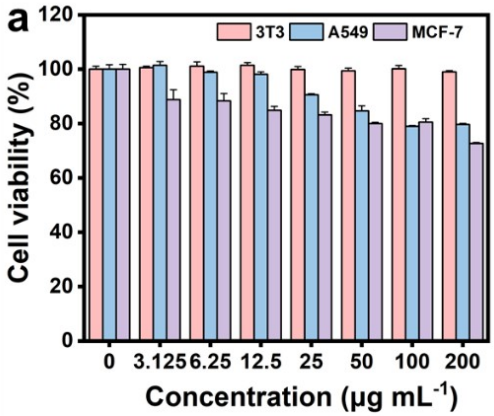

Fig. S33 Cell viability after 48 h incubation with HA@$Bi_2(SeO_3)_3$ NSs at different concentration. n = 3.

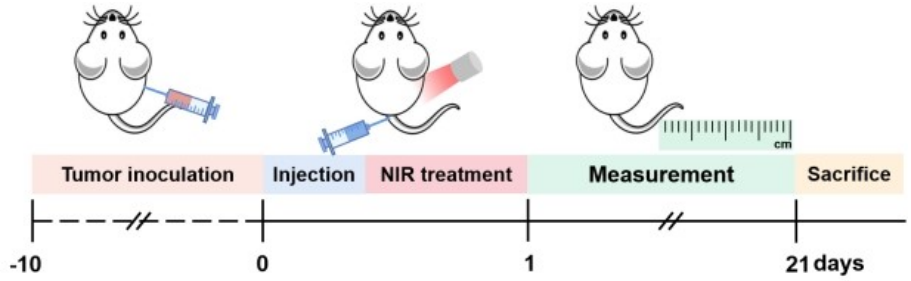

Fig. S34 Work flow for treatment of MCF-7 tumour-bearing mice using HA@$Bi_2(SeO_3)_3$ NSs.

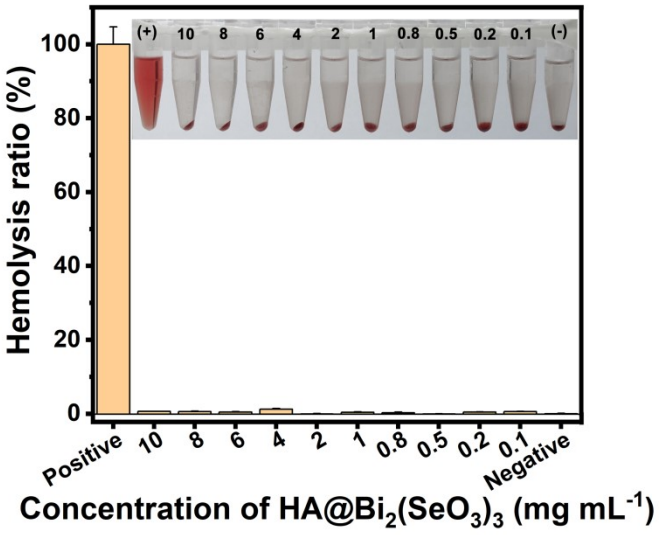

Fig. S35 Hemolysis analysis of the as-prepared HA@$Bi_2(SeO_3)_3$ NSs.

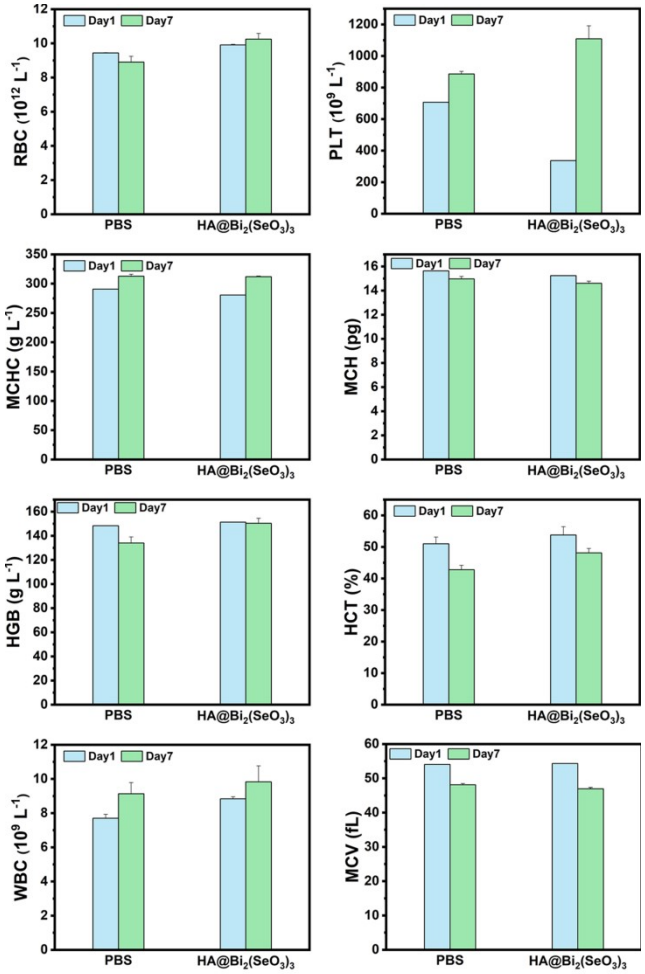

Fig. S36 Blood routine analysis of the HA@$Bi_2(SeO_3)_3$ NS-treated mice.

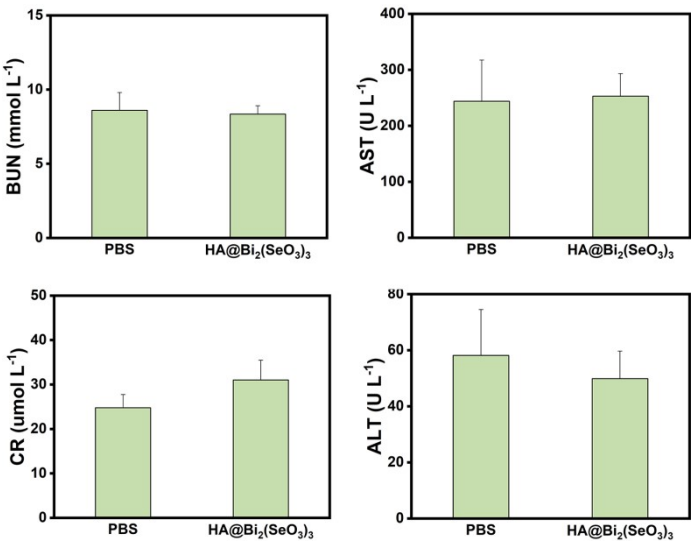

Fig. S37 Blood biochemistry analysis of the HA@$Bi_2(SeO_3)_3$ NS-treated mice.

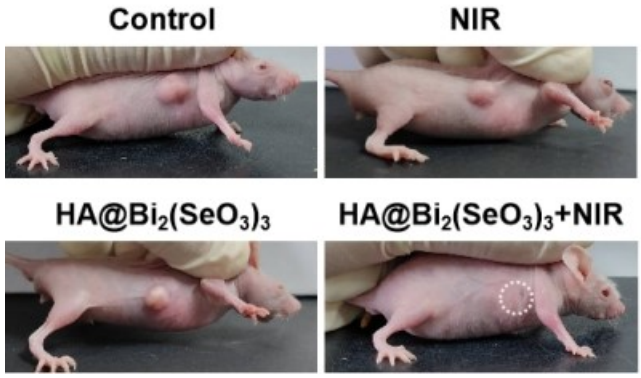

Fig. S38 Representative images on 21th day of MCF-7 tumour-bearing mice after different treatments.

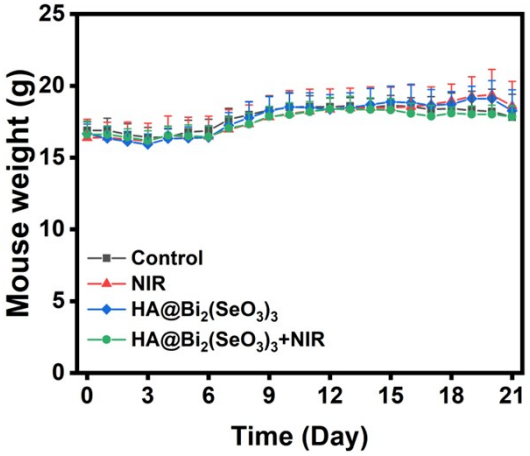

Fig. S39 Body weight curves of tumour-bearing mice after different treatments.

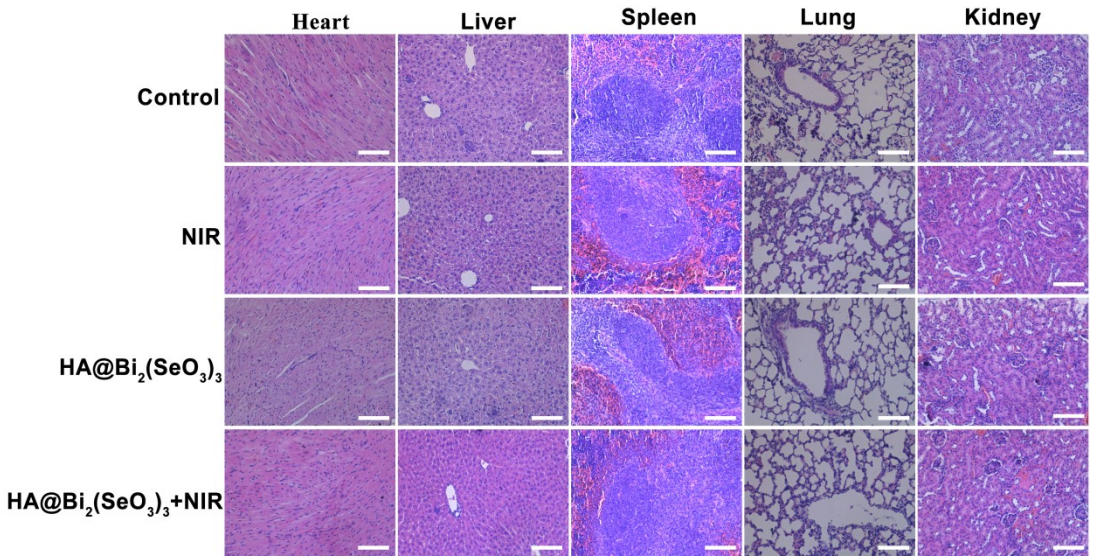

Fig. S40 Representative images of H&E staining of vital organs after different treatments. Scale bar = 100 μm.

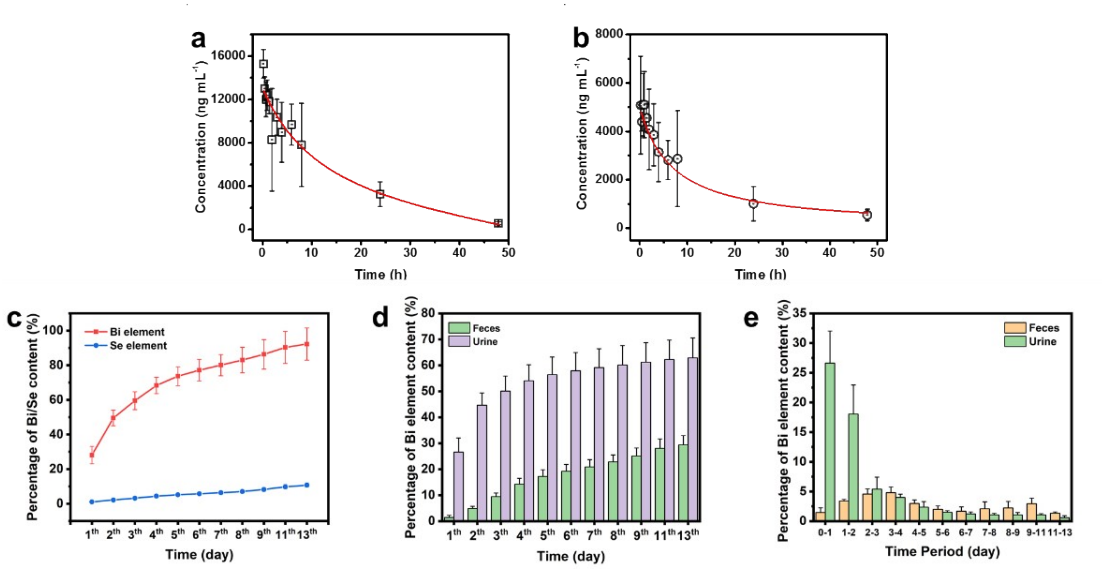

Fig. S41 ICP-MS results of bismuth/selenium element in the plasma and excreta of the raised mice.

To investigate the biodegradation and bioelimination profile of the nanosheets, we used ICP-MS to quantify the bismuth and selenium element in the plasma and excreta of the raised mice. According to the ICP-MS results of plasma sample (Fig. S41a-b), $HA@Bi_2(SeO_3)_3$ NSs exhibited a rapid blood clearance with 8.37 h half-life for bismuth and 5.16 h for selenium element, and the elimination rate are 0.10 L h^{-1} kg^{-1} and 0.35 L h^{-1} kg^{-1}, respectively. According to the quantification results of the two elements in excreta including feces and urine (Fig. S41c), approximately 90.3 % bismuth element was eliminated on the 11^{th} day after the intravenous injection of $HA@Bi_2(SeO_3)_3$ NSs, while only 9.8 % of selenium element was eliminated. Since bismuth is the signature element that does not exist inside body, the results demonstrated that a majority of the as-prepared nanosheets was eliminated within two weeks, and major of the selenium element was absorbed and utilized by the body. According to the respective results of

bismuth element quantification in feces and urine (Fig. S41d), urine is the leading way of elimination, and the amount of the eliminated bismuth through urine was at least 2.1-fold, average for one day, more than feces. Moreover, the amount of bismuth eliminated through urine reaches maximum value in the first day, while that in feces in the fourth day (Fig. S41e). These results suggest that redundant/underutilized nanosheets could be eliminated rapidly through metabolism and thereby can decrease the toxicity of the nanosheets. Since selenium is a necessary micronutrient in body, the amount of selenium that was absorbed yet not eliminated might play an important role in supporting the daily activity of body.

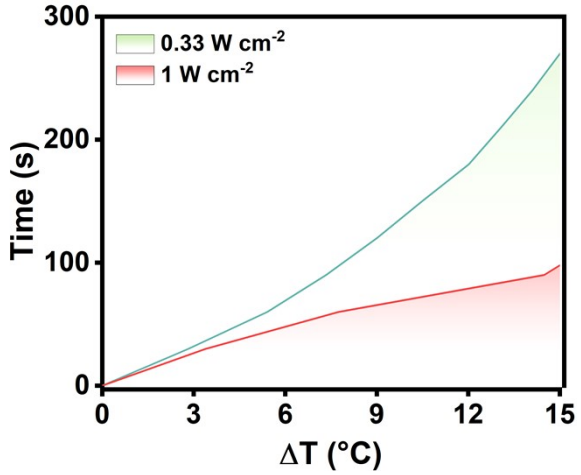

Fig. S42 Feasibility proof of 808 nm laser with 0.33 W cm^{-2} as the maximal permissible exposure according to the American National Standard for Safe Use of Lasers (ANSIZ136.1−2014).[2] When the increasing temperature was set as 15 °C (cells die rapidly owing to microvascular thrombosis and ischaemia at 46−52 °C), 90 s was required for 1 W cm^{-2} while 270 s for 0.33 W cm^{-2}.

Reference

1 C. Dai, S. Zhang, Z. Liu, R. Wu, and Y. Chen, Two-Dimensional Graphene Augments Nanosonosensitized Sonocatalytic Tumour Eradication, *ACS Nano,* 2017, **11**, 9467-9480.

2 Y. Yang, X. Fan, L. Li, Y. Yang, A. Nuernisha, D. Xue, C. He, J. Qian, Q. Hu, H. Chen, J. Liu, and W. Huang, Semiconducting Polymer Nanoparticles as Theranostic System for Near-infrared-II Fluorescence Imaging and Photothermal Therapy under Safe Laser Fluence, *ACS Nano,* 2020, **14**, 2509-2521.